RESEARCH ARTICLE | MARCH 19 2024

Interpreting pore-scale fluctuations: Predicting transport coefficients in multiphase flow through porous media using the Green–Kubo formulation—An experimental investigation

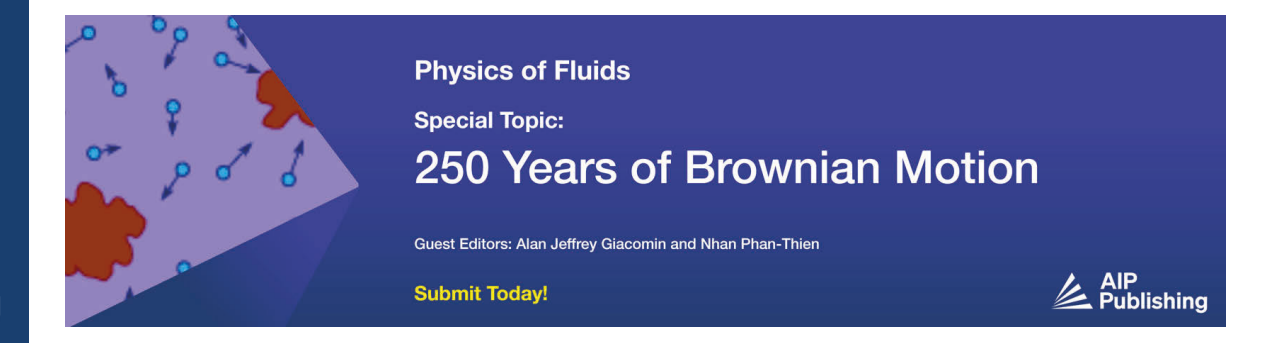
Umar Alfazazi <sup>(1)</sup>; Dick Bedeaux <sup>(1)</sup>; Signe Kjelstrup <sup>(1)</sup>; Marcel Moura <sup>(1)</sup>; Mohammad Ebadi <sup>(1)</sup>; Peyman Mostaghimi <sup>(1)</sup>; James E. McClure <sup>(1)</sup>; Ryan T. Armstrong <sup>(2)</sup>



Physics of Fluids 36, 036616 (2024) https://doi.org/10.1063/5.0185605









# Interpreting pore-scale fluctuations: Predicting transport coefficients in multiphase flow through porous media using the Green-Kubo formulation—An experimental investigation

Cite as: Phys. Fluids **36**, 036616 (2024); doi: 10.1063/5.0185605 Submitted: 31 October 2023 · Accepted: 21 February 2024 · Published Online: 19 March 2024







Umar Alfazazi, 1 Dick Bedeaux, 2 Digne Kjelstrup, 2 Digne Marcel Moura, 3 Digne Mohammad Ebadi, 1 Deyman Mostaghimi, 1 Dignes E. McClure, 4 Dignes T. Armstrong Dignes Dignes E. McClure, 4 Dignes T. Armstrong Dignes Dignes E. McClure, 4 Dign

## **AFFILIATIONS**

- <sup>1</sup>School of Civil and Environmental Engineering, The University of New South Wales, Sydney, Australia
- <sup>2</sup>PoreLab, Department of Chemistry, Norwegian University of Science and Technology, Trondheim 7491, Norway
- <sup>3</sup>PoreLab, the Njord Center, Department of Physics, University of Oslo, Oslo 0316, Norway

## **ABSTRACT**

Flow fluctuations that are commonly associated with multiphase flow in porous media are studied using concepts from non-equilibrium thermodynamic and statistical mechanics. We investigate how the Green–Kubo formulation of the fluctuation dissipation theorem can be used to predict the transport coefficient from the two-phase extension of Darcy's law. Flow rate-time series data are recorded at the millisecond time-scale using a novel experimental setup that allows for the determination of flow fluctuation statistics. By using Green–Kubo relations, a transport coefficient is predicted based on the integrated autocorrelation function. Notably, this coefficient aligned closely with the total effective phase mobility computed using Darcy's equation for multiphase flow, particularly in scenarios where a linear relationship between flow rate and pressure gradient was observed. Our results open a new field of coefficient explorations where microscale fluctuations during multiphase flow are directly linked to macroscale parameters.

© 2024 Author(s). All article content, except where otherwise noted, is licensed under a Creative Commons Attribution (CC BY) license (http://creativecommons.org/licenses/by/4.0/). https://doi.org/10.1063/5.0185605

## I. INTRODUCTION

In the last decade, there have been notable observations of fluid fluctuations that occur during multiphase flow in porous media, particularly at low Capillary numbers. <sup>1-4</sup> Intermittent flow and fluctuations influence the energy dissipation on the continuum-scale via the relative permeability. <sup>5</sup> Recently, Winkler *et al.* <sup>6</sup> investigated two-phase flow fluctuations in a pore network model using the fluctuation dissipation theory (FDT) from Green–Kubo (G-KB). While the correlation of the fluctuating contribution from G-KB was reported and Onsager symmetry was observed, the measurements were neither compared to the relative permeability, nor were they experimentally validated. Herein, we address these issues by studying a simplified experimental system where multiphase flow fluctuations can be observed at the millisecond timescale.

In the late nineties, Yuan et al.<sup>7.8</sup> reported pressure fluctuations during slow-rate mercury injection capillary pressure experiments in

cores. They found the pressure fluctuations to be a result of different degrees of constriction along the pore paths. DiCarlo *et al.*9 demonstrated acoustic and hydroacoustic fluctuations during drainage and imbibition experiments. Rapid fluctuation events were reported during drainage and found to be related to discrete fluid bursts, as opposed to imbibition experiments which had limited fluctuation events. Overall, in these studies, the flow process, pore structure, and interfacial tension were shown to influence the degree to which pressure fluctuations were observed.

Recently, pore-scale experiments using synchrotron-based x-ray microcomputed tomography (micro-CT) have opened a new domain for researchers to better understand fluid-fluid-rock interactions at the pore-level during multiphase flow in porous media. <sup>10,11</sup> Complex pore-scale events have been taken as the cause of intermittent flow behavior based on 3D images of fluid distributions. <sup>1,3,4,12-14</sup>

<sup>&</sup>lt;sup>4</sup>National Security Institute, Virginia Tech, Blacksburg, VA 24061, USA

<sup>&</sup>lt;sup>a)</sup>Author to whom correspondence should be addressed: ryan.armstrong@unsw.edu.au

Here, intermittency is observed as dynamic occupancy of a pore by one immiscible fluid and then another over a periodic timescale.

At the continuum scale, Rücker *et al.*<sup>15</sup> conducted steady state (SS) experiments to relate pore-scale fluctuations with core-scale behavior using sandstone and sintered-glass samples. They observed fluctuations in differential pressure ( $\Delta P$ ), fluid saturations, and resistivity readings. Additionally, the  $\Delta P$  fluctuations were found to follow a Gaussian distribution and were not associated with experimental noise. The observed fluctuations were found to be at the capillary energy scale suggesting that fluctuations were caused by pore-scale events. Similar studies were conducted to investigate pore-scale intermittent fluid dynamics on large (centimeter-scale) core samples. They showed pressure fluctuations with higher amplitude in experiments conducted at medium and low capillary number (Ca) and reported a non-Gaussian (non-symmetric) distribution.

Pressure fluctuations have been investigated by performing power spectral analysis using Fourier transformation.  $^{5,16}$  By transforming the pressure fluctuations from the time domain to the frequency domain, red-noise scaling was observed where the observed fluctuations are found to occur at various frequencies during the flow process. The study demonstrated a cascade of timescales for multiphase flow experiments at SS. Spurin *et al.* <sup>17</sup> also performed power spectral analysis of  $\Delta P$  fluctuations by using a continuous wavelet transformation and highlighted the limitation of Fourier transformations used in their earlier work. They found that the spectral power depends on the frequency of the fluctuations, size of the sample, and rock heterogeneity. In addition, analysis done by Rücker *et al.* and McClure *et al.*  $^{15,18}$  showed that non-thermal fluctuations play an important role in multiphase flow phenomena and constrain the validity of the multiphase extension of the Darcy's law.

The study of fluctuations in other physical systems using methods from statistical physics is not new. Hauge and Martin-Löf<sup>19</sup> derived the Langevin equation from fluctuating hydrodynamics. Other examples include studies of non-equilibrium fluctuations in molecular motors<sup>20</sup> and studies in the field of earth sciences to measure transport coefficients and viscosity of molten silicates at different pressures.<sup>21</sup> The G-KB formula predicts that fluctuations observed during multiphase flow are related to the overall permeability, and the measurements suggest that this is true. The question is how precisely the prediction is linked to the observation.

In reservoir engineering, multiphase flow in porous media is typically modeled by the empirical extension of Darcy's equation, as shown in Eq. (1).<sup>11</sup> The Darcy's law takes the familiar form of a linear constitutive model with the transport determined by the effective permeability.<sup>22</sup> This was first established by Wyckoff and Botset,<sup>23</sup> where they studied the flow of gas and liquid mixtures in unconsolidated sands,

$$\overrightarrow{u_i} = -\frac{k_i K}{\eta_i} \left( \nabla P - \rho \, \overrightarrow{g} \right), \tag{1}$$

where  $u_i$  is the Darcy velocity (m/s) of phase  $i, k_i$  is relative permeability of phase i, K is the absolute permeability (m²),  $\eta_i$  is fluid dynamic viscosity (Pa s) of phase  $i, \nabla P$  is pressure gradient (Pa/m),  $\rho$  is fluid density (kg/m³), and g is acceleration due to gravity (m/s²). Equation (1) presents a linear relationship between  $u_i$  and  $\nabla P$ . However, recent observations of intermittent flow behavior show that there can be a non-linear correlation between these two parameters. This happens under a capillary force dominated flow regime  $^{3,16,25,26}$ 

and can be understood as a threshold to flow. Capillary barriers lead to slow fluctuations, and long timescales are necessary to perform experiments that reach stationary conditions.

During multiphase flow in porous media, the dynamic changes in fluid-configurations leads to flow fluctuations caused by pore-scale events. 6,15,27 These fluctuations are mechanical in nature, but we now propose that they share similarities with the thermal fluctuations at the molecular level. 6,18,28 So far, this assumption has not been studied before.

Thermal fluctuations at the molecular level can be predicted statistically based on a Gaussian distribution, as explained above. These are connected to a transport coefficient in G-KB theory. The G-KB theory is an inherent part of the theory of non-equilibrium or irreversible thermodynamics. It is an expression of time-reversal invariance or microscopic reversibility. This hypothesis assumes that the probability to observe, on the average, that a fluctuation in some property i at time t is followed by another fluctuation j after a time lag  $\tau$ , is equal to the probability to observe the reverse situation, that the fluctuation j at time t, is followed by the fluctuation i after a time lag  $\tau$ . In addition, the regression hypothesis is assumed, stating that a system subject to a small deviation from its equilibrium state will return to its original equilibrium state, by a linear law, which is the same on the molecular- and the macroscopic level.

The G-KB relation has been used for various applications to predict transport coefficients.<sup>21,30</sup> However, it has never been used to predict permeabilities in porous media. Winkler et al.6 made a first approach to decompose athermal fluctuations of porous media flows using non-equilibrium thermodynamics. By defining a suitable representative elementary volume (REV) where the ergodic assumption and the assumption of microscopic reversibility hold,<sup>31</sup> they showed that the steady state flow fluctuations were Gaussian. Additionally, the integral of the cross correlation functions became symmetric, in line with Onsager's reciprocal relation. McClure et al.30 also investigated the non-equilibrium thermodynamics of two-phase flows of immiscible fluids in porous media using time-and-space averaging and demonstrated that valid transport coefficients can be obtained provided that there is no net work performed by fluctuating models. This assumption is less restrictive compared to the assumption that fluctuations obey a Gaussian distribution.

They studied correlation functions for flow fluctuations of wetting and nonwetting components. In the current work, we investigate whether FDT can provide insight into the transport behavior (permeability) of two-phase flow in porous media. In contrast to Winkler *et al.*, 6 we provide experimental results and compare the outcomes from FDT with the standard expressions derived from Darcy's law for multiphase flow using the concept of relative permeability. Previous studies have not compared G-KB theory with the linear law for multiphase flow.

# II. MATERIAL AND METHODS

# A. Experimental system and experiments

Steady state experiments were conducted on a sintered glass sample with dimensions of 6 mm length and 3 mm diameter. The experiments were conducted at different constant differential pressures while monitoring the total flow rate at the outlet using a mass flow meter. The approach we adopted is different from the conventional technique of performing steady state experiments, where fluids are co-injected

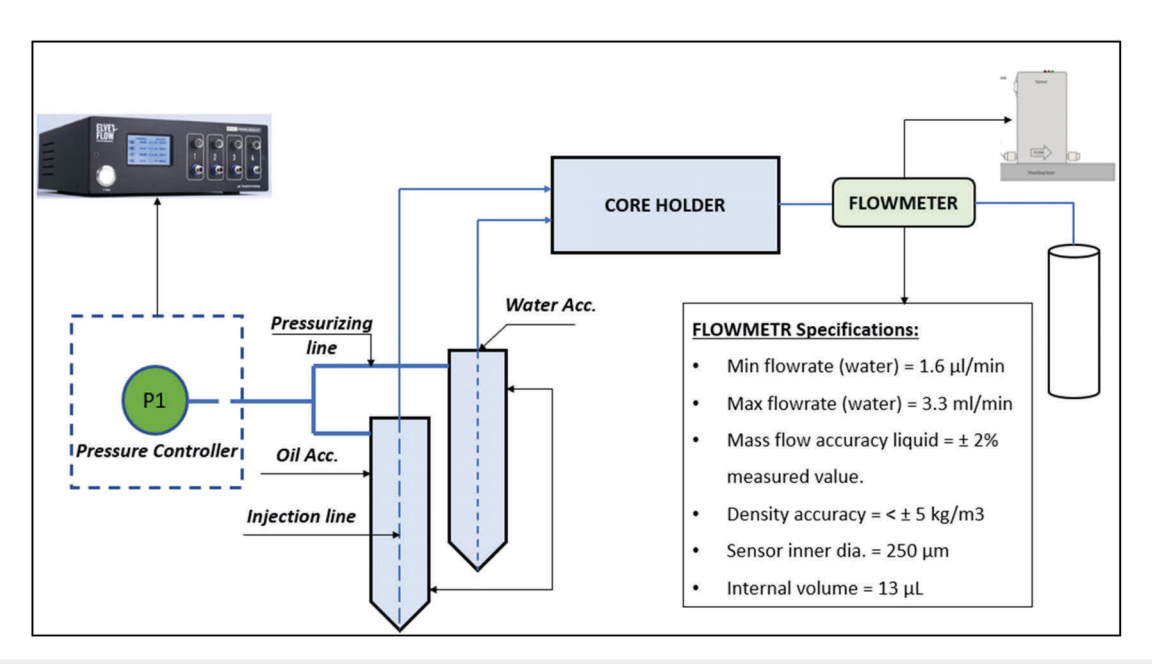


FIG. 1. Schematic of the core flooding setup used for measuring flow fluctuations under a constant pressure gradient.

under constant flow rates condition. Our novel approach measures the flux fluctuations under a constant gradient. The experiments were conducted by using DI-water and decane as the wetting and non-wetting phases, respectively. *In situ* fluid saturation from x-ray CT scanning was not recorded during our experiments. A schematic of the core flooding setup used is shown in Fig. 1. It consists of a pressure regulator, two fluid accumulators, core holder, flow meter, a fractional collector, and a logging device. Short and precise lines and fittings were used to avoid leakages and pressure losses. Initially, the sample was fully saturated by injecting several pore volumes (PVs) of DI-water under a high-pressure gradient. Water absolute permeability was then calculated at different pressure drops and found to be approximately  $10 \pm 1$  Darcy, equivalent to  $9.9 \pm 0.9 \times 10^{-12} \, \mathrm{m}^2$ .

Co-injection experiments were conducted at constant inlet pressures controlled by a pressure controller from ELVEFLOW. The pressure controller can provide unique performance with pressure stability

and pressure resolution of 0.005% and 0.003% full scale (FS), respectively. Fluids were simultaneously injected at a water fractional flow of roughly 50% ( $\rm F_w\sim0.5$ ) and at different inlet pressures. Based on the injection pressures, corresponding  $\it Ca$  were calculated by using Eq. (2), as reported by Spurin  $\it et al.^{14}$  Details of the experimental parameters are summarized in Table I,

$$Ca = \frac{q_t}{\gamma \left(\frac{1 - f_w}{\eta_n} - \frac{f_w}{\eta_w}\right)},\tag{2}$$

where Ca is the dimensionless Capillary number,  $q_t$  is Darcy's average total flux (m/s),  $\gamma$  is interfacial tension between the wetting and non-wetting phases (N/m), and  $f_w$  is water fractional flow.

A mass flow meter by BRONKHORST was connected at the core holder outlet, and the total flow rate was measured at an interval of 30 ms. The mass flow meter provides accurate readings within  $\pm 2\%$ 

**TABLE I.** Summary of calculated parameters during the 2-phase flow experiments.

Pressure drop (psi)	Pressure drop (Pa)	Average flux (m/s)	Capillary number, Ca	Linear law coefficient (m²/Pa s)	Average integral ACF (m <sup>2</sup> /s)	Average F (1/Pa)
1.5	10 342	$1.96 \times 10^{-5}$	$4.91 \times 10^{-6}$		$8.28 \times 10^{-12}$	1.33
2.0	13 790	$2.36 \times 10^{-5}$	$6.32 \times 10^{-6}$		$8.84 \times 10^{-12}$	1.24
2.5	17 237	$3.18 \times 10^{-5}$	$7.96 \times 10^{-6}$	$1.09 \times 10^{-11}$	$8.68 \times 10^{-12}$	1.27
3.0	20 684	$3.94 \times 10^{-5}$	$9.51 \times 10^{-6}$		$5.71 \times 10^{-12}$	1.93
4.0	27 579	$5.07 \times 10^{-5}$	$1.27 \times 10^{-5}$		$5.17 \times 10^{-12}$	2.14
5.0	34 474	$5.91 \times 10^{-5}$	$1.48 \times 10^{-5}$	$8.19 \times 10^{-12}$	$3.39 \times 10^{-12}$	2.42
5.5	37 921	$6.51 \times 10^{-5}$	$1.63 \times 10^{-5}$	$8.75 \times 10^{-12}$	$3.99 \times 10^{-12}$	2.22
6.0	41 369	$6.91 \times 10^{-5}$	$1.73 \times 10^{-5}$	$7.74 \times 10^{-12}$	$3.84 \times 10^{-12}$	2.09
7.0	48 263	$7.80 \times 10^{-5}$	$1.96 \times 10^{-5}$	$6.81 \times 10^{-12}$	$3.12 \times 10^{-12}$	2.25
8.0	55 158	$8.48 \times 10^{-5}$	$2.12 \times 10^{-5}$	$6.81 \times 10^{-12}$	$2.98 \times 10^{-12}$	2.29

accuracy of the measured value. Conducting steady state experiments using this setup and approach facilitated the measurement of flow fluctuations (at milliseconds), utilized in the application of fluctuation dissipation theorem. To capture the fluctuations from each reading, the following steps were considered. First, only data recorded after achieving steady state were used for analysis. This implies that the macroscopic variables fluctuate around well-defined and constant averages. 32 To ensure the attainment of a steady-state flow, both fluids were simultaneously injected at a 50:50 ratio for over 50 pore volumes (PV). Second, only the fluctuations were considered by subtracting the mean average from the time series data. We assumed that the fluctuations were representative of the intermittency between the water and oil phase fluxes. Based on the fluctuation time series in the data, we computed a probability density function (PDF) using kernel density estimation (KDE) technique, which computed a normalized PDF of the dataset, using the MATLAB function KernelDistribution. The autocorrelation function (ACF) was then determined using the MATLAB function autocorr. An average of three runs was taken at each pressure drop tested. One should note that all three runs (for each of the pressure drops) were consistent and within acceptable error range as will be shown in Sec. III.

For further analysis, the ACF curve was then fitted to an exponential decay function by using the least squares method. We, therefore, assumed that only the zero-frequency response of the ACF was required for all subsequent calculations. The implication of this assumption is considered within Sec. III. Consequently, the integral of the ACF was determined based on the area under the fitted curve. The integral of the ACF was necessary for prediction of the transport coefficient using FDT as will explained in Sec. II B.

## B. Thermodynamic description of relative permeability

In non-equilibrium thermodynamics theory (NET), the set of fluxes and their corresponding driving forces (gradients) are defined by the system's entropy production. Here, we consider two component fluxes, driven by a pressure gradient. There are two routes for determination of transport coefficients, representative of porous media permeabilities: (1) the linear flux-force relations and (2) the G-KB formulation of the fluctuation dissipation theorem (FDT). The fluxforce relations are linear when the system response is proportional to the gradients that drive the fluxes. Such responses are described in the simplest way in familiar equations for heat-, mass-, charge-, and volume-transport, i.e., Fourier's, Fick's, Ohm's, and Darcy's law, respectively.<sup>33</sup> The FDT represents more complex relationships when porous media are concerned.<sup>34</sup> The definition of the REV average variables is central. The FDT can then be used to relate fluctuations in steady state flows to the system's permeability coefficients. Hence, FDT establishes a connection between the small fluctuations in a system and its macroscopic behavior. The FDT has been applied successfully in homogeneous solutions. 35,36 Herein, our aim is to present a comparative analysis; using linear (Darcy) law as well as FDT to determine the overall transport coefficient for two-phase fluid flow in porous medium.

The two sets of equations (linear law and FDT) for determination of permeabilities have a common root in the entropy production of the system. The entropy production in isothermal porous medium has in the outset two terms, one for each fluid (wetting and non-wetting phase, *w* and *n*). In a discrete isothermal porous system at constant

composition (saturation), with the *x*-direction as the direction of net transport, the entropy production is given by

$$\sigma = -J_w \frac{1}{T} \frac{\Delta \mu_w}{\Delta x} - J_n \frac{1}{T} \frac{\Delta \mu_n}{\Delta x}.$$
 (3)

Here,  $\mu_i$  (i = w, n) is the chemical potential of the wetting and non-wetting fluids in J, T is temperature in K,  $J_i$  is the particle flux of component i in m<sup>-2</sup> s<sup>-1</sup>. In the present experiments at steady state with two-phase co-injection, constant temperature, and constant concentration, the chemical potential difference throughout the system,  $\Delta \mu_i$ , simplifies

$$\Delta \mu_i = V_i \Delta p,\tag{4}$$

where  $V_i$  (i=w,n) is the partial volume per particle of component i in  $m^3$ , and  $\Delta p$  is hydrostatic pressure difference between the two sides of the system. It should be noted that the force-flux relations are formulated with the pressure gradient component of the chemical potential while neglecting the concentration gradient part. Nevertheless, the diffusive fluxes are accounted for through pressure diffusion, in addition to viscous phenomena. Furthermore, the characteristic times of the experiment reflect these phenomena; hence, there is no additional timescale for diffusion to report. We can vary the total flow and the fractional composition of the flows. For the REV,

$$J_{w} = -L_{ww} \frac{1}{T} \frac{\Delta \mu_{w}}{\Delta x} - L_{wn} \frac{1}{T} \frac{\Delta \mu_{n}}{\Delta x} = -\frac{1}{T} (L_{ww} V_{w} + L_{wn} V_{n}) \frac{\Delta p}{\Delta x},$$
 (5a)

$$J_n = -L_{nw} \frac{1}{T} \frac{\Delta \mu_w}{\Delta x} - L_{nn} \frac{1}{T} \frac{\Delta \mu_n}{\Delta x} = -\frac{1}{T} (L_{nw} V_w + L_{nn} V_n) \frac{\Delta p}{\Delta x}, \quad (5b)$$

where  $L_{ww}$ ,  $L_{wn}$ ,  $L_{nw}$ , and  $L_{nn}$  are coefficients that quantify the relationship between the thermodynamic forces and the resulting fluxes. Their values reflect the properties of the system. In the context of fluid flow through porous medium, they characterize how easily the fluid flows. Following Onsager, the conductivity matrix is symmetric. The coefficients are functions of state variables and reflect different types of mechanisms for flow, i.e., ganglion dynamics, viscous flow, diffusion, etc. While the main coefficients are connected to Darcy's or Fick's law, viscous flow, or diffusion, respectively, the coupling coefficients are related to energy storage or depletion. The storage and depletion terms are interesting for the characterization of mechanisms. Darcy's velocities for wetting and non-wetting phases are then written as

$$u_w = V_w J_w = -\frac{1}{T} (V_w L_{ww} V_w + V_w L_{wn} V_n) \frac{\Delta p}{\Delta x} = -\frac{k_w K}{n_w} \frac{\Delta p}{\Delta x}, \quad (6a)$$

$$u_n = V_n J_n = -\frac{1}{T} \left( V_n L_{nw} V_w + V_n L_{nn} V_n \right) \frac{\Delta p}{\Delta x} = -\frac{k_n K}{\eta_n} \frac{\Delta p}{\Delta x}, \quad (6b)$$

where  $k_i$  is the relative permeability of fluid i (i = w, n) and K is the absolute permeability,  $\eta_i$  is fluid viscosity i (i = w, n). The average volumetric flux,  $J_V$ , as measured by our mass flow meter, is given by

$$J_{V} = u_{w} + u_{n}$$

$$= V_{w}J_{w} + V_{n}J_{n}$$

$$= -\frac{1}{T}(V_{n}L_{ww}V_{w} + V_{w}L_{wn}V_{n} + V_{n}L_{nw}V_{w} + V_{n}L_{nn}V_{n})\frac{\Delta p}{\Delta x}$$

$$= -\frac{1}{T}L_{VV}\frac{\Delta p}{\Delta x} = -\left[\frac{k_{w}}{\eta_{w}} + \frac{k_{n}}{\eta_{n}}\right]K\frac{\Delta p}{\Delta x}.$$
(7)

The final term comes from Darcy's law [Eq. (1)] by adding the Darcy velocities for each phase and assuming no gravitational potential.

Based on Eq. (7), the main transport coefficient  $L_{VV}$  can be related to the phase mobilities from 2-phase Darcy, which is given by

$$\frac{L_{VV}}{T} = \left[ \frac{k_w}{\eta_w} + \frac{k_n}{\eta_n} \right] K,\tag{8}$$

where  $L_{VV}$  is the transport coefficient attached with the pressure gradient  $\Delta P/\Delta x$ ,  $\left[\frac{k_w}{\eta_w} + \frac{k_u}{\eta_n}\right] K$  is a product of the relative and absolute permeability terms and viscosities (yielding an effective mobility for both phases) based on Eq. (1) with no gravitational force. In summary, Eq. (8) can be used for determining the transport coefficient  $L_{VV}$  based on the linear flux–force approach highlighted earlier.

The fluxes in the linear flux–force relations are time average fluxes over the REV cross section. On the molecular level, the fluxes have fluctuating contributions,  $J_{i,R}$ , the average of which is zero. In NET, the correlations of the fluctuating contributions are given by the FDT<sup>34</sup> as shown by

$$\left\langle J_{i,R}(t)J_{j,R}(t')\right\rangle = \frac{2k_BL_{ij}}{V_I}\delta(t-t').$$
 (9)

The left-hand side of Eq. (9) expresses the correlation of two particle fluxes, the first taking place at t, and the second taking place at t'. The  $k_{\rm B}$  is the Boltzmann constant and  $L_{ij}$  are the symmetric Onsager coefficients for the two fluctuating phenomena,  $(L_{ij} + L_{ji}) = 2L_{ij}$ . The expression has been integrated over the volume  $V_L$ , which we do not know *a priori*. The timescale and the range over which the fluctuating contributions are correlated is small compared to those of the average fluxes. The correlations may, therefore, be described by delta-functions. The flux of each component that is considered in Eq. (9), yielding auto- or cross correlations.

In our experimental setup, we measure the total volume flux  $J_V$  only. This provides a single coefficient for transport, due to autocorrelations of the volume flux  $(J_V = V_w J_w + V_n J_n)$ . Equation (9) is then written as

$$\langle J_{V,R}(t)J_{V,R}(t')\rangle = \frac{2k_BL_{VV}}{V_I}\delta(t-t').$$
 (10)

The left-hand side of Eq. (10) gives the autocorrelation function. The right-hand side contains  $L_{VV}$ , i.e., the transport coefficient that represents the total volume flux in our experiments. Note that we do not specify any of the cross-coefficients in Eq. (10). By integrating Eq. (10) over time t, we obtain

$$\frac{2k_B L_{VV}}{V_I} = \int_{t'}^{\infty} dt \langle J_{V,R}(t) J_{V,R}(t') \rangle. \tag{11}$$

For t < t' the integrand is zero. The correlation function  $\langle J_{V,R}(t)J_{V,R}(t')\rangle$  depends only on t-t'. The foundation of Eq. (11) lies in Onsager's regression hypothesis, asserting that the regression of fluxes on the microscale is equivalent to that on the macroscale, i.e., the time of the experiment. We assume that this holds true.

We see that the strength of the correlations determines the Onsager coefficient. Boltzmann's constant enters because the integration in principle takes place over all the molecular fluctuations and relaxation times. This means that a timescale from femtoseconds and

up is involved. In practice, experimental time correlations of shorter time scales are not observable due to limitations in an instrument's temporal resolution. The implications of this will be discussed in Sec. III. At this point, we propose a practical ratio between that measured by the linear law and that measured by the FDT.

By introducing  $L_{VV}/T$ , we obtain a practical ratio,

$$F = \frac{L_{VV}/T}{\int_{t'}^{\infty} dt \left\langle J_{V,R}(t)J_{V,R}(t') \right\rangle} = \frac{V_L}{2k_B T}.$$
 (12)

The F is the pre-factor (1/Pa), containing  $V_L$ , T, and  $k_B$ . The integral is taken from the shortest timescale that can be observed with the apparatus used. The  $L_{VV}$  is the coefficient of the linear law,  $\int_{t'}^{\infty} dt \left\langle J_{V,R}(t)J_{V,R}(t') \right\rangle$  is the integral of the time-correlation function. The prefactor is essential for predicting  $L_{VV}$  from FDT. Indeed, F would be particular for each porous media and experimental setup.

In this study, we computed the transport coefficient,  $L_{VV}$ , from the linear (Darcy) law, i.e., using the RHS of Eq. (7). We also solved for F, which can be used for predicting a transport coefficient from FDT as explained above. Our assumption is that the linear law and the GKB relation provide the same result. The shortest timescale available in the DFT study was 30 ms, and the measured fluctuations relate to the total volumetric flux,  $J_V$ , only. Therefore, our setup did not allow for the evaluation of correlations below 30 ms nor the determination of the cross correlation coefficients, i.e.,  $L_{ij}$ .

To summarize; this study seeks to understand if the FDT, as expressed in Eq. (12), provides valuable insights into the transport behavior of the two-phase fluids in porous media, and how the FDT results compare to Darcy's law total effective mobility, as presented in Eq. (7).

# **III. RESULTS AND DISCUSSION**

The experimental results are summarized in Table I. The experiments were conducted at Ca between  $4.9 \times 10^{-6}$  and  $2 \times 10^{-5}$ . All measurements were conducted at pressure drops within the capillary dominated flow regime. Figure 2 shows the measured relationship between the average flux with respect to pressure drop. Figure 2 highlights measured points (highlighted in blue color) for a regime with linear behavior. The regression line for the experiments was forced to

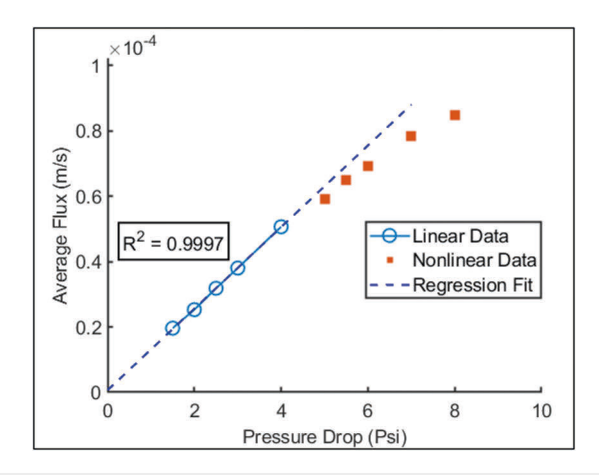


FIG. 2. Relationship between measured average flux and pressure drop.

go through zero. At low pressure drops (1.5–4 psi), the linear relationship between the average flux and pressure drops has an  $\rm R^2=0.9999$ . Hence, this obeys Darcy's law. At higher pressure drops (above 5 psi), there was a systematic deviation from the linear trend with a more pronounced effect at 7 and 8 psi. This deviation represents the onset of non-linearity, i.e., non-Darcy behavior. No threshold value was observed on the low-pressure drop side. Thus, in our experiments, the Darcy law regime applied until a pressure drop of 4 psi, which is equivalent to Ca =  $1.27\times10^{-5}$ . As the pressure drop increased (increased Ca), we come outside this regime. More elaborate methods are then needed to decompose data in the non-Darcy regime.

The non-Darcy behavior was most evident at the two highest pressure drops tested, giving  $Ca = 1.96 \times 10^{-5}$  and  $2.12 \times 10^{-5}$ . Gao et al.<sup>3</sup> showed similar behavior using a mini-core sample of Bentheimer sandstone. They observed non-linear behavior at  $Ca \approx 10^{-5}$  which correlated with rapid sub-minute changes in fluid configurations in their reported 3D images. Similar observations have also been reported by other authors<sup>3,16,37</sup> where a power-law relation has been proposed at a capillary dominated flow regime. Gao et al.<sup>3</sup> suggested that at a critical Ca, there is intermittent flow because of increased flow conductance compared to Darcy's flow. Note that the non-Darcy flow behavior is different from the flow described during viscous dominated flow.<sup>11</sup>

The results presented in Fig. 2 were utilized to determine the coefficient  $L_{VV}$  using Eqs. (7) and (8), through two different approaches. The first approach involved considering the initial points where the linear effect was observed and calculating the average flux vs pressure drop. This fitting was forced to pass through the origin. Consequently, this slope was valid only up to a pressure drop of 4 psi, as shown in Fig. 2. When a non-linear effect was observed, i.e., between a pressure drop of 5–8 psi, the slope is calculated locally for each experimental measurement. The local slope was determined using a midpoint finite difference method. We therefore assume that a linear response would still occur over a small change in the pressure drop. All calculated slopes (coefficient) are summarized in Table I and reported as a total effective mobility, see Eq. (8).

Next, we analyzed the fluctuations from the measured total flux at different pressure drops. Figures 3(a) and 3(b) are typical examples of time series of flux fluctuations for 1.5 and 8 psi, respectively. The statistical frequency of the flux was also measured by plotting the probability density function (PDF) of the flux fluctuation, as shown in Figs. 3(c)-3(f). The flux fluctuation, as depicted in the figures, is determined by subtracting the mean of the flux data from the original flux data. In other words, flux fluctuation is calculated as follows: flux fluctuation  $= flux \, data - mean(flux \, data)$ . We conducted triplicate runs at each pressure drop to test repeatability. It is evident from the figures that there was consistency between the experiments; only a slight difference was seen attributable to experimental inaccuracies. Additionally, we observed two defined trends from the PDF distribution. First, there was a bimodal distribution (non-Gaussian), with two peaks observed. The bimodal distribution was more pronounced at the lower pressure drops. Second, there was the presence of a long tail, especially when the pressure drop was increasing. In their study, Rücker et al. 15 demonstrated that the fluctuation histograms are not symmetric and exhibit a bimodal distribution. However, the non-Gaussian pattern of the averages becomes increasingly symmetric. The non-Gaussian behavior could be related to different mechanisms taking place during

flow over a wide range of time scales. Similarly, Wang *et al.* <sup>16</sup> observed that the PDF of the measured pressure fluctuations had a non-symmetric distribution. Our results, however, contrasted with the findings of Winkler *et al.*, <sup>6</sup> who found that fluctuations in their flow time series data were Gaussian.

Our paper incorporates the non-Gaussian nature of the fluctuation distributions to characterize these fluctuations. At the molecular level, these distributions are nearly Gaussian. However, on the molecular level, a shift away from Gaussian behavior is expected, particularly when the system is not in equilibrium. It appears that two phenomena are superimposed, resulting in a bimodal distribution. By averaging over the experiment, the tails shown in the Figs. 3(c)–3(f) become less significant. In other words, the tails do not have weight in the analysis. In summary, the underlying assumption that allows us to derive the Green–Kubo relations is the assumption of local equilibrium. However, it is anticipated that this assumption may not hold true when the driving force becomes too large.

It is worth mentioning that plotting the probability density functions (PDFs) on a linear-log scale enables a clearer demonstration of the long tail decay relative to the flux fluctuations, as presented in the supplementary material (Fig. S13). Additionally, we analyzed the stationarity of the flux data for all experiments by dividing the time series data into separate segments and calculate the mean and variance of each segment. If the means and variances of different segments of the time series vary significantly, it suggests non-stationarity in the data, which could also indicate inconsistencies in the data recording. The time series was found to be nearly stable, with a slight variance change observed among the three data segments. This slight variation could be attributed to minor experimental artifacts, as expected. A detailed analysis of stationarity can be found in the supplementary material (Table S1).

Given consistent PDF results from the repeated experiments, F was calculated based on Eq. (12), which is a function of the coefficient  $L_{VV}$  and the integral of the ACF. The integral of the ACF was calculated by determining the area under the ACF curve. For a more simplistic approach, the ACF curve was fitted with an exponential decline function using the least squares method before computing the integral. We therefore consider only the zero-frequency response of the ACF.

It is worth noting that the calculation of the integral of the ACF, the experimental ACF curves (original ACF) yielded inconsistent results for the high Ca flows due to fluctuations in the ACF, as shown in Figs. 4(a)-4(c). This effect was most pronounced at higher Ca flows (as pressure drop increases) while a zero-frequency response that decays to zero was observed for the lower Ca flows. To verify the consistency of the results when fitting the ACF to a zero-frequency model, the ACF fitting that followed by integration was conducted for three different time intervals (0-500,0-1000, and 0-2000 s). The results were consistent with only small differences (less than 1%) for all time intervals, as presented in the supplemental material. Based on the consistency of the analysis, all ACF curves and subsequent integrations of the ACF presented herein were based on using a time interval of 0-1000 s.

Figures 4(a)–4(c) are typical examples of the ACF analysis conducted by comparing the experimentally measured ACF (original ACF) to the fitted ACF at 1.5, 4, and 8 psi, respectively. Similar analyses were conducted for all measured pressure drops (see supplemental material). At low pressure drops of 1.5, 2, and 2.5 psi, the fitted ACF line matched the original ACF curve. However, as the pressure drop increases, the fitting does not perfectly match the original ACF [as

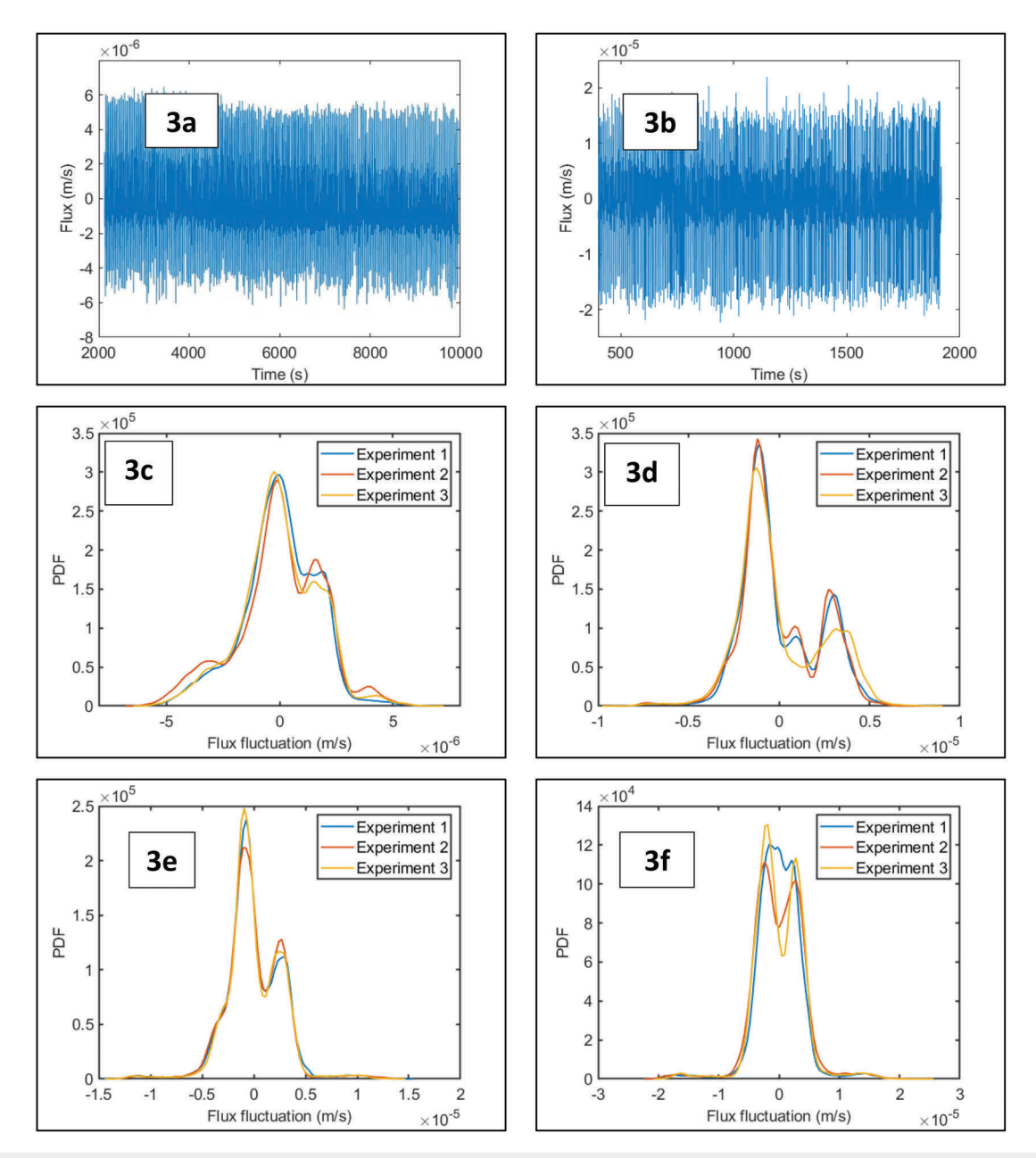
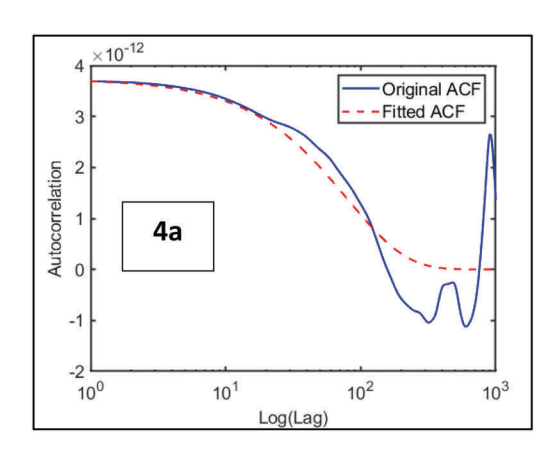
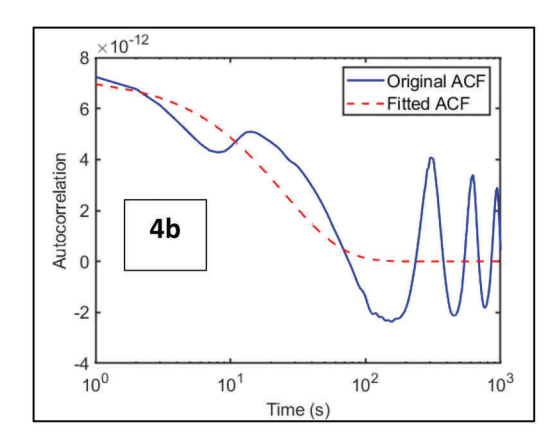


FIG. 3. Time series plots of total flux as a function of time for different pressure drops; (a) 1.5, (b) 8 psi. PDF distribution as a function of total flux at different pressure drops; (c) 1.5, (d) 3, (e) 5, and (f) 8 psi. Measurements are shown for triplicate experiments.

observed in Figs. 4(b) and 4(c)], which suggests that other responses in addition to the zero-frequency response could be relevant. It is evident from Figs. 4(b) and 4(c) that there is an increasing presence of oscillations at the initial part of the experimentally measured ACF curves, i.e., between time  $10^0$  and  $10^1$  s. These oscillations are absent during the lowest pressure drops at similar time intervals, as shown in Fig. 4(a). Consequently, the fitting, which is based on a simple model, does not fully match the original ACF at higher pressure drops. In other words, the model performs better when there are no oscillations

in the ACF curve. As a result, the integral of the fitted ACF at higher pressure drops are affected by the model's inability to capture the oscillations in the experimentally measured ACF's. The increasing presence of the oscillations could be attributed to a memory effect caused by different flow regimes or modes of transport operating at different spectral frequencies, which was increasingly observed as the pressure drop was increased. Such oscillations could also be related to saturation waves as observed by Rücker *et al.* Is during steady state (SS) coinjection experiments. The development of sufficient models to





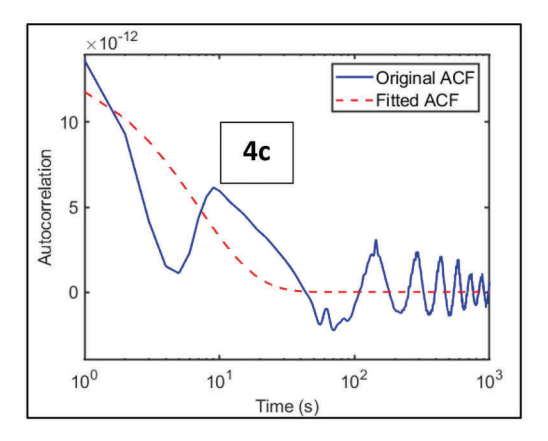


FIG. 4. ACF analysis based on the measured time series data at different pressure drops showing the measured ACF and fitted ACF curves. (a) ACF analysis for 1.5 psi, (b) ACF analysis for 4 psi, and (c) ACF analysis for 8 psi.

capture such memory effect will require additional work. Inadequate statistics in ACF evaluations, stemming from a limited number of replicable readings (only three conducted for each pressure drop), could also lead to increased oscillations in the ACFs. Given the time required to conduct an experiment, simulation studies are better suited for a larger number of replicate studies, which could be used in the future to supplement our experiment works.

The prefactor, F, was calculated for each pressure drop as shown in Fig. 5. At the lowest pressure drops, it was evident that F was approximately constant and roughly around 1.2 (1/Pa). As the pressure drop increased (corresponding to 3-8 psi), F jumped to around 1.9 (1/Pa). Figure 5 can be further explained based on the ACF analysis shown in Figs. 4(a)-4(c): at the lowest pressure drops [Fig. 4(a)], the fitting is matching with the original ACF resulting in a prefactor of approximately 1 (1/Pa). This becomes inconsistent at higher pressure drops primarily due to increased oscillations in the ACF as explained earlier. It is also worth highlighting that, despite pressure drops between 1.5 and 4 psi falling within the linear-Darcy region, as shown in Fig. 2, the presence of the fluctuations at 3 and 4 psi in the ACF curves resulted in a prefactor of approximately 2 (1/Pa). This effect was likely due to the inability of the exponential decay function to capture the oscillating ACF trend. It is worth noting that all drop experiments with oscillations in their ACF resulted in similar

prefactor values given the standard deviation associated with the measurement.

As established earlier, F is a practical ratio that gives insight into the prediction of transport coefficient based on FDT. To predict the transport coefficient using FDT, F must be known from an independent measurement. Herein, we see that F was 1.3 at the lowest pressure drops (1.5 and 2.5 psi) considering experimental errors. However, F increased to 2.2 (1/Pa) as pressure drop is increased from 3 and 8 psi. At low pressure drops between 1.5 and 2.5 psi, the zero-frequency model matches the experimental ACF well, whereas at higher pressure drop the zero-frequency model does not match the experimental ACF well. These observations suggest that additional responses (frequencies) play a role, which needs to be the focus of future work. Our current results suggest that the FDT can predict total effective phase mobility with a prefactor of approximately unity for low Ca flows when the ACF displays a zero-frequency response.

Transport coefficients using the G-KB relation are typically determined by starting with fluctuations at the molecular level and, thus, integrating the autocorrelation function from femtoseconds and up. <sup>21</sup> At a timescale of millisecond, as used here (30 ms sampling time), all actual fluctuations cannot be fully captured. Here, the fluctuations at time scales smaller than milliseconds were not captured. Figure 6(a) (re-produced based on ACF plot shown by Karki and Stixrude<sup>21</sup>)

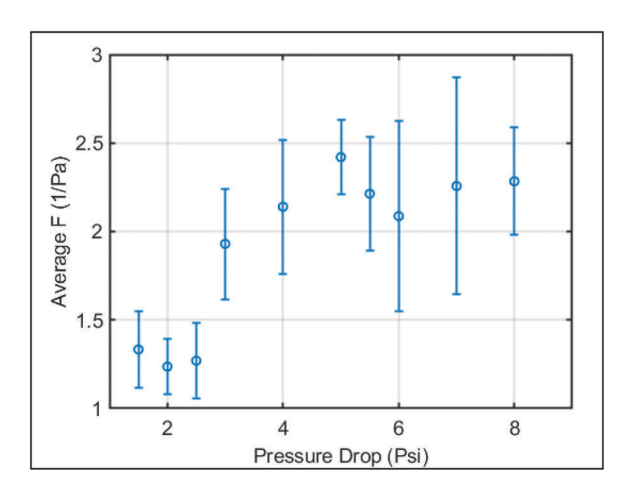


**FIG. 5.** Relationship between average prefactor F (1/Pa) and pressure drop (psi) calculated based on G-KB. Error bars are standard deviations taken from triplicate experiments.

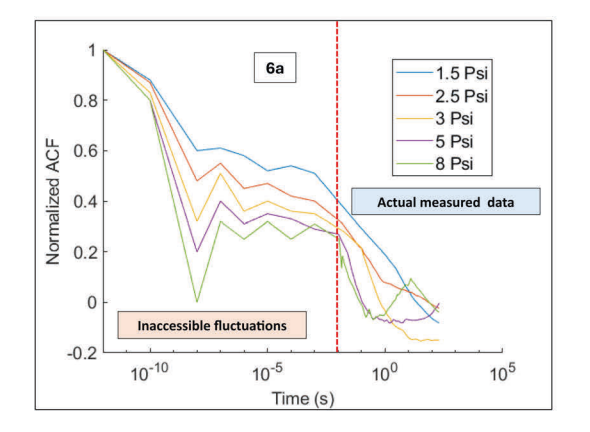
shows a typical ACF plot that captures all molecular fluctuations. The missing part of the autocorrelated time series in our experiment is highlighted as a hypothetical realization. Because of this issue, we instead proposed a practical ratio (or prefactor), F which is particular for a given porous media and experimental setup. Therefore, considering the RHS of Eq. (12), we could replace  $k_B$  with  $\kappa_B$ , reflecting a possible non-thermal behavior of the fluctuations, when the formula is applied for porous medium, resulting in

$$F = \frac{L_{VV}/T}{\int_{t}^{\infty} dt \langle J_{V,R}(t)J_{V,R}(t') \rangle} = \frac{V_L}{2\kappa_B T}.$$
 (13)

The factor F is particular for each porous media and experimental setup. Such an approach has some resemblance to the statistical mechanical application to granular media, which also has an effective Boltzmann constant, defined as  $\kappa_B = 1.39$  Future work could focus on the determination of F for different rock types, technological

developments to measure higher frequency fluctuations, and/or theoretical developments to deal with the missing frequencies.

Figure 6(b) shows the time correlation functions of the lag time as a function of the pressure drop used. Depending on the pressure drop, the decay in the ACF profile varies. Initially, there is a sudden decay of the auto correlation during a short timescale. This is followed by slow logarithmic decay, which is more pronounced at higher pressure drop and increases as the pressure drop is increasing. Finally, there is slow decay in the ACF over much longer time scales. Furthermore, fluctuations in the ACF are observed and become more pronounced as the pressure drop increases. Additionally, the fluctuations are minimal at low pressure drops, but appear periodic at higher pressure drops. Such periodic fluctuations could be related to memory effects, which could result from different flow regimes or periodic modes of energy transfer. For example, capillary energy could be accumulated in the system and then released in a periodic manner over a timescale longer than a single fluid-fluid displacement event. These processes may influence the flow behavior and could affect phase mobilities. These potential memory effects warrant further investigations. Such long-term memory effect may influence the flow behavior depending on the amplitude of the fluctuating production at this scale. Based on spectral power analysis, Spurin et al.  $^{17}$  showed that  $\Delta P$  fluctuations at both low and high periods/frequencies can play a role in large scale flow properties. The small contributions can be attributed to non-linear flow dynamics that may play a role in continuum scale flow properties. Memory was also observed as periodic saturation waves by Rücker et al. 14 Yet the correlation of the fluctuating contribution needs to be considered in comparison with the larger earlier timescale contributions that also contribute to the transport coefficient. Future work will study the aspect of memory observed in the reported AFCs. In addition, a new theoretical approach needs to be developed to handle memory effects when the G-KB relation is used. Additional analysis will be conducted to assess the oscillations and nonstationarity observed in the auto-correlation functions (ACFs). This will involve the application of common parametric spectral approaches, including wavelet transformation, dynamic mode decomposition (DMD), and autoregressive moving average (ARMA). 17,40,41 Additionally, stochastic adaptive estimators, such as the Kalman filter, recursive least mean squares, and least squares, will be employed. 42



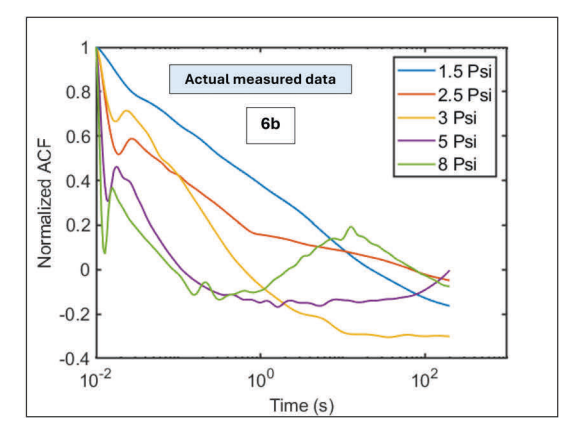


FIG. 6. (a) Time Autocorrelation function of flow fluctuations highlighting fluctuations at the molecular scale. The first part of the figure indicates the timescale and corresponding inaccessible fluctuation that cannot be measured due to system limitation. (b) Actual ACF calculated at different at different pressure drops. The actual measurements were recorded at 30 ms intervals.

#### IV. CONCLUSIONS

Our aim was to contribute to the development of a deeper understanding of transport phenomena in porous media and open new possibilities for predicting and characterizing fluid flow in such systems. To this end, transport coefficients determined by linear flux–force relations were compared to those determined by the G-KB formulation of the fluctuation dissipation theorem. By determining the prefactor correctly, the coefficient  $L_{VV}$  could possibly be calculated for different experiments at different fractional flow regimes. Herein, we provide the first experimental evidence of using the FDT to determine  $L_{VV}$  when F is independently measured. Further work is indeed required to test different porous systems under a range of different fractional flows and flow regimes.

We studied fluctuations in steady-state flows in porous media involving two incompressible immiscible phases, employing concepts from non-equilibrium thermodynamics and statistical mechanics. We showed that the Green-Kubo theory can be used to describe the transport coefficient (total effective mobility) based on the autocorrelation function of the fluctuating flux. The time-dependent function showed a dependency on the experimentally tested pressure drops. The decay in the ACF was found to be fast at low pressure drop while there were periodic fluctuations (memory) in the ACF at higher pressure drops. Additionally, the periodic fluctuations in the ACF were not perfectly captured using the zero-frequency model. The periodic fluctuations are presumably due to memory effects and their impact on transport properties should be considered in future work. The fluctuations could also be attributed to inadequate statistics, potentially leading to increased ACF fluctuations, given that only three replicates' measurements were conducted for each pressure drop. In the future, simulations studies are likely better suited to evaluate the larger number of replicate studies required to study ACF fluctuations.

Provided that the ACF displays a zero-frequency response, which occurred at low Ca flows, the prefactor F was nearly unity, meaning that the transport coefficient of the linear Darcy law regime and the transport coefficient of the FDT from the G-KB theory yielded that same result. The fundamental implications of the F being nearly unity at low Ca flows and increasing for higher Ca warrants further investigations. Finally, the memory effects could explain the erratic behavior observed in our pre-factor, F, outside the linear Darcy law regime. The G-KB approach presented herein did not consider memory effects nor cross correlation functions. Further theoretical developments will be required for systems where memory effects are observed in the ACF. Further experimental advancements will be required for the determination of cross correlation functions.

# SUPPLEMENTARY MATERIAL

See the supplementary material section for the additional results that, although not incorporated into the main body of the manuscript, contribute further perspectives to our study. The supplementary material includes supplementary figures detailing the calculation of integral ACF from the measured flow-time series data for all reported pressure drops.

## **ACKNOWLEDGMENTS**

U.A. is grateful for his tuition fee scholarship from the University of New South Wales, Sydney. R.T.A. acknowledges his

Australian Research Council Future Fellowship (FT210100165). D. B., S.K., and M.M. are grateful to the Center of Excellence Funding Scheme of the Research Council of Norway, Project No. 262644 Porelab. M.M. also acknowledges the support of the Researcher Project for Young Talents Funding Scheme of the Research Council of Norway, Project No. 324555.

## **AUTHOR DECLARATIONS**

#### **Conflict of Interest**

The authors have no conflicts to disclose.

#### **Author Contributions**

Umar Alfazazi: Data curation (equal); Formal analysis (equal); Investigation (equal); Methodology (equal); Validation (equal); Visualization (equal); Writing – original draft (equal). Dick Bedeaux: Conceptualization (equal); Formal analysis (equal); Funding acquisition (equal); Writing – review & editing (equal). Signe Kjelstrup: Conceptualization (equal); Formal analysis (equal); Funding acquisition (equal); Writing – review & editing (equal). Marcel Moura: Formal analysis (equal); Writing – review & editing (equal). Mohammad Ebadi: Software (equal); Writing – review & editing (equal). Peyman Mostaghimi: Supervision (equal); Writing – review & editing (equal). James E. McClure: Conceptualization (equal); Writing – review & editing (equal); Formal analysis (equal); Funding acquisition (equal); Methodology (equal); Project administration (equal); Resources (equal); Supervision (equal); Writing – review & editing (equal).

# **DATA AVAILABILITY**

The data that supports the findings of this study are available within the article and its supplementary material.

# **REFERENCES**

- <sup>1</sup>C. A. Reynolds, H. Menke, M. Andrew, M. J. Blunt, and S. Krevor, "Dynamic fluid connectivity during steady-state multiphase flow in a sandstone," Proc. Natl. Acad. Sci. U. S. A. 114, 8187 (2017).
- <sup>2</sup>Y. Gao, A. Qaseminejad Raeini, M. J. Blunt, and B. Bijeljic, "Pore occupancy, relative permeability and flow intermittency measurements using x-ray microtomography in a complex carbonate," Adv. Water Resour. 129, 56 (2019).
- <sup>3</sup>Y. Gao, Q. Lin, B. Bijeljic, and M. J. Blunt, "Pore-scale dynamics and the multiphase Darcy law," Phys. Rev. Fluids 5, 013801 (2020).
   <sup>4</sup>C. Spurin, T. Bultreys, B. Bijeljic, M. J. Blunt, and S. Krevor, "Mechanisms con-
- <sup>4</sup>C. Spurin, T. Bultreys, B. Bijeljic, M. J. Blunt, and S. Krevor, "Mechanisms controlling fluid breakup and reconnection during two-phase flow in porous media," Phys. Rev. E **100**, 043115 (2019).
- <sup>5</sup>C. Spurin, M. Rücker, M. Moura, T. Bultreys, G. Garfi, S. Berg, M. J. Blunt, and S. Krevor, "Red noise in steady-state multiphase flow in porous media," Water Resour. Res. 58, e2022WR031947, https://doi.org/10.1029/2022WR031947 (2022).
- <sup>6</sup>M. Winkler, M. A. Gjennestad, D. Bedeaux, S. Kjelstrup, R. Cabriolu, and A. Hansen, "Onsager-symmetry obeyed in athermal mesoscopic systems: Two-phase flow in porous media," Front. Phys. **8**, 60 (2020).
- <sup>7</sup>H. H. Yuan, "Pore-scale heterogeneity from mercury porosimetry data," SPE Form. Eval. **6**, 233 (1991).
- 8H. Yuan and B. Swanson, "Resolving pore-space characteristics by rate-controlled porosimetry," SPE Form. Eval. 4, 17 (1989).
- <sup>9</sup>D. A. DiCarlo, J. I. G. Cidoncha, and C. Hickey, "Acoustic measurements of pore-scale displacements," Geophys. Res. Lett. **30**, 17 (2003).
- 10 T. Bultreys, S. Van Offenwert, W. Goethals, M. N. Boone, J. Aelterman, and V. Cnudde, "X-ray tomographic micro-particle velocimetry in porous media," Phys. Fluids 34, 042008 (2022).

- <sup>11</sup>M. J. Blunt, Multiphase Flow in Permeable Media: A Pore-Scale Perspective (Cambridge University Press, 2017).
- <sup>12</sup>C. Spurin, T. Bultreys, M. Rücker, G. Garfi, C. M. Schlepütz, V. Novak, S. Berg, M. J. Blunt, and S. Krevor, "Real-time imaging reveals distinct pore-scale dynamics during transient and equilibrium subsurface multiphase flow," Water Resour. Res. 56, e2020WR028287, https://doi.org/10.1029/2020WR028287 (2020).
- <sup>13</sup>Y. Gao, Q. Lin, B. Bijeljic, and M. J. Blunt, "X-ray microtomography of intermittency in multiphase flow at steady state using a differential imaging method," Water Resour. Res. 53, 10274, https://doi.org/10.1002/2017WR021736 (2017).
- <sup>14</sup>C. Spurin, T. Bultreys, M. Rücker, G. Garfi, C. M. Schlepütz, V. Novak, S. Berg, M. J. Blunt, and S. Krevor, "The development of intermittent multiphase fluid flow pathways through a porous rock," Adv. Water Resour. 150, 103868 (2021).
- <sup>15</sup>M. Rücker, A. Georgiadis, R. T. Armstrong, H. Ott, N. Brussee, H. van der Linde, L. Simon, F. Enzmann, M. Kersten, and S. Berg, "The origin of non-thermal fluctuations in multiphase flow in porous media," Front. Water 3, 671399 (2021).
- <sup>16</sup>S. Wang, C. Spurin, and T. Bultreys, "Pore-scale imaging of multiphase flow fluctuations in continuum-scale samples," Water Resour. Res. 59, e2023WR034720, https://doi.org/10.1029/2023WR034720 (2023).
- <sup>17</sup>C. Spurin, R. T. Armstrong, J. McClure, and S. Berg, "Dynamic mode decomposition for analysing multi-phase flow in porous media," Adv. Water Resour. 175, 104423 (2023).
- <sup>18</sup>J. E. McClure, S. Berg, and R. T. Armstrong, "Capillary fluctuations and energy dynamics for flow in porous media," Phys. Fluids 33, 083323 (2021).
- <sup>19</sup>E. H. Hauge and A. Martin-Löf, "Fluctuating hydrodynamics and Brownian motion," J. Stat. Phys. 7, 259 (1973).
- <sup>20</sup>E. Ben-Isaac, Y. Park, G. Popescu, F. L. H. Brown, N. S. Gov, and Y. Shokef, "Effective temperature of red-blood-cell membrane fluctuations," Phys. Rev. Lett. 106, 238103 (2011).
- <sup>21</sup>B. B. Karki and L. P. Stixrude, "Viscosity of MgSiO<sub>3</sub> liquid at Earth's mantle conditions: Implications for an early magma ocean," Science 328, 740 (2010).
- <sup>22</sup>J. E. McClure, M. Fan, S. Berg, R. T. Armstrong, C. F. Berg, Z. Li, and T. Ramstad, "Relative permeability as a stationary process: Energy fluctuations in immiscible displacement," Phys. Fluids 34, 092011 (2022).
- 23R. D. Wyckoff and H. G. Botset, "The flow of gas-liquid mixtures through unconsolidated sands," J. Appl. Phys. 7, 325 (1936).
- <sup>24</sup>M. Muskat and M. W. Meres, "The flow of heterogeneous fluids through porous media," J. Appl. Phys. 7, 346 (1936).
- 25K. T. Tallakstad, H. A. Knudsen, T. Ramstad, G. Løvoll, K. J. Måløy, R. Toussaint, and E. G. Flekkøy, "Steady-state two-phase flow in porous media: Statistics and transport properties," Phys. Rev. Lett. 102, 074502 (2009).

- <sup>26</sup>Y. Zhang, B. Bijeljic, Y. Gao, Q. Lin, and M. J. Blunt, "Quantification of nonlinear multiphase flow in porous media," Geophys. Res. Lett. 48, e2020GL090477 (2021).
- 27R. T. Armstrong, J. E. McClure, M. A. Berrill, M. Rücker, S. Schlüter, and S. Berg, "Beyond Darcy's law: The role of phase topology and ganglion dynamics for two-fluid flow," Phys. Rev. E 94, 043113 (2016).
- <sup>28</sup>D. Bedeaux and S. Kjelstrup, "Fluctuation-dissipation theorems for multiphase flow in porous media," Entropy 24, 46 (2021).
- <sup>29</sup>R. Kubo, "The fluctuation-dissipation theorem," Rep. Prog. Phys. 29, 255 (1966).
- 30). E. McClure, S. Berg, and R. T. Armstrong, "Thermodynamics of fluctuations based on time-and-space averages," Phys. Rev. E 104, 035106 (2021).
- <sup>31</sup>M. Erpelding, S. Sinha, K. T. Tallakstad, A. Hansen, E. G. Flekkøy, and K. J. Måløy, "History independence of steady state in simultaneous two-phase flow through two-dimensional porous media," Phys. Rev. E 88, 053004 (2013).
- <sup>32</sup>F. Lanza, S. Sinha, A. Hansen, A. Rosso, and L. Talon, "Transition from viscous fingers to foam during drainage in heterogeneous porous media," Phys. Fluids 35, 103119 (2023).
- <sup>33</sup>K. Signe, B. Dick, J. Eivind, and G. Joachim, Non-Equilibrium Thermodynamics for Engineers, 2nd ed. (World Scientific, 2010).
- <sup>34</sup>D. Bedeaux, S. Kjelstrup, and S. K. Schnell, Nanothermodynamics: Theory and Applications (World Scientific, 2023).
- 355 X. Liu, T. J. H. Vlugt, and A. Bardow, "Predictive darken equation for Maxwell-Stefan diffusivities in multicomponent mixtures," Ind. Eng. Chem. Res. 50, 10350 (2011).
- <sup>36</sup>F. Bresme and J. Armstrong, "Note: Local thermal conductivities from boundary driven non-equilibrium molecular dynamics simulations," J. Chem. Phys. 140, 016102 (2014).
- <sup>37</sup>Y. Gao, A. Q. Raeini, M. J. Blunt, and B. Bijeljic, "Dynamic fluid configurations in steady-state two-phase flow in Bentheimer sandstone," Phys. Rev E 103, 013110 (2021).
- <sup>38</sup>C. Spurin, G. G. Roberts, C. P. B. O'Malley, S. Krevor, M. J. Blunt, and H. Tchelepi, "Pore-scale fluid dynamics resolved in pressure at the Darcy scale," Geophys. Res. Lett. 50(18), e2023GL104473, https://doi.org/10.1029/2023GL104473 (2023).
- 39S. F. Edwards and R. B. S. Oakeshott, "Theory of powders," Physica A 157, 1080 (1989)
- <sup>40</sup>E. Isufi, A. Loukas, A. Simonetto, and G. Leus, "Autoregressive moving average graph filtering," IEEE Trans. Signal Process. 65, 274 (2017).
- graph Intering, TEEE Trans. signal Process. 03, 274 (2017).
   M. A. Benjamin, R. A. Rigby, and D. M. Stasinopoulos, "Generalized autoregressive moving average models," J. Am. Stat. Assoc. 98, 214 (2003).
- 42B. P. Gibbs, Advanced Kalman Filtering, Least-Squares and Modeling: A Practical Handbook (Wiley, 2011).